3

Defect Engineering During Czochralski Crystal Growth and Silicon Wafer Manufacturing

Lukáš Válek[1,2] and Jan Šik[1]
[1]*ON Semiconductor Czech Republic,*
[2]*Institute of Physical Engineering,*
Brno University of Technology,
Czech Republic

1. Introduction

Single crystal silicon has played the fundamental role in electronic industry since the second half of the 20th century and still remains the most widely used material. Electronic devices and integrated circuits are fabricated on single-crystal silicon wafers which are produced from silicon crystals grown primarily by the Czochralski (CZ) technique. Various defects are formed in the growing crystal as well as in the wafers during their processing. This chapter deals with the topic of engineering of crystal defects in the technology of manufacturing silicon single crystals and silicon wafers for the electronic industry. A basic overview of crystal defects found in semiconductor-grade silicon is provided and mechanisms of their formation are introduced. The impact of crystal defects on the manufacturing and performance of electronic devices is outlined and some of the methods of defect analyses are described. Finally, the most important methods for control of defect formation are summarized.

2. Industrial production of silicon for electronics

Single crystals of silicon for today´s electronic industry are produced primarily by the Czochralski (CZ) method (Czochralski, 1918; Teal & Little, 1950). Only applications with extreme demands on pure bulk material utilize the float zone (FZ) method (Keck & Golay, 1953). The CZ method is based on crystal pulling from the melt, while the FZ method utilizes recrystallization of polysilicon rod which is locally molten by passage of the RF coil. The processes differ mainly in production cost and speed, which favor the CZ method, and in the purity of produced material, which is higher in case of the FZ method. The lower purity, which was seemingly unfavorable, helped CZ silicon become the dominant material as it makes silicon wafers more resistant against thermal stress and metallic contamination. Furthermore the FZ process could not follow the continual increase in crystal diameter. The diameter of 200 mm is the current size limit for FZ crystals while 450 mm capability was demonstrated for CZ process. As the chapter deals mainly with CZ silicon, the CZ crystal growth will be more closely described.

2.1 Czochralski growth of silicon crystals

Today´s Czochralski (CZ) grown silicon single crystals are produced in a mass scale in diameters of up to 300 mm, but the 150 mm and 200 mm processes are still considered as standard. A typical CZ puller is shown in Fig. 1. The puller consists of an upper and lower chamber formed by steel water-cooled shells. The lower chamber contains a graphite hot zone with active central part and thermally insulating outer parts. A silica crucible is placed in the heart of the hot zone which is supported by a graphite susceptor on the pedestal attached to the lower shaft. The seed holder is fastened onto the upper shaft (or affixed to a cable). The heater is a meandering-coil element heated by high electric current. Both chambers are piped to a vacuum system. The puller is typically purged with inert gas (usually argon). In the beginning of the process the quartz crucible is loaded with a charge of polysilicon chunks and the single crystalline seed is fitted into the seed holder. After closing the puller the chambers are evacuated and re-filled by inert gas to the desired process pressure. The process starts with melting the polysilicon charge by applying high power to the heater. Once the charge is molten, the melt flow is stabilized under steady conditions and the seed is lowered towards the melt. After the seed is dipped into the melt, the system is adjusted to achieve a stable interface between the melt and the seed crystal. Pulling the seed upwards crystallizes the melt at the solid-liquid interface and the crystal proceeds to grow.

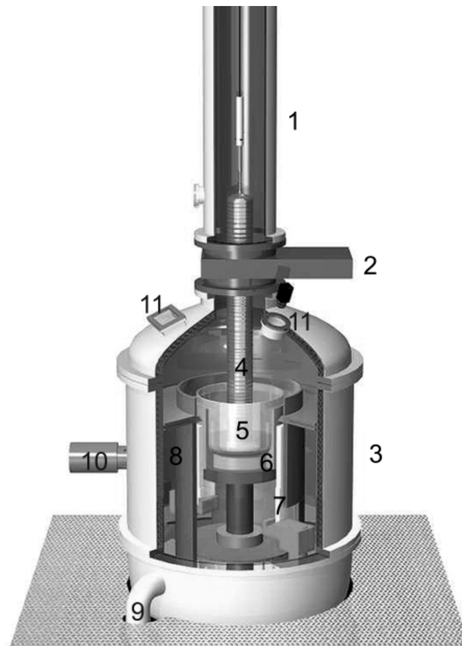

Fig. 1. A typical configuration of a CZ silicon puller. (1) Upper chamber, (2) isolation valve, (3) lower chamber, (4) grown crystal, (5) silica crucible, (6) graphite susceptor, (7) heater, (8) insulation, (9) vacuum pipe, (10) heater pyrometer window, (11) operator and camera windows.

Once the seed touches the melt surface, it is subjected to a huge thermal shock leading to generation of numerous dislocations. In order to achieve dislocation-free growth, "necking" is performed. To achieve this condition, the crystal pulling rate is increased to about 3 to 6 mm per minute, and the crystal diameter is reduced to about 5 to 2 mm, which allows dislocations to partially freeze in the neck and partially move to the crystal surface. Dislocation-free growth is usually achieved after several centimeters of the neck growth. Then the pulling rate is significantly decreased and the diameter is slowly increased. The crystal grows into the form of a cone called the crown. As the diameter increases to the desired crystal diameter the pull rate is gradually increased (the so called "shouldering stage") until the crystal grows with the desired diameter and the proper growth rate. Then, the cylindrical portion of the crystal, the "crystal body", is grown.
The melt and the crystal are in intimate contact at the solid-liquid interface. The melt surface forms a meniscus to the crystal which reflects the light from the hot crucible to the chamber windows. This results in the appearance of a shiny ring on the melt surface around the crystal. As the meniscus height increases with crystal radius, changes in the meniscus height can be sensed and used for crystal diameter control during the growth of the crystal body. Another option for crystal diameter control is a measurement of the meniscus diameter with a CCD camera. The crystal diameter is controlled by the pulling rate and simultaneously the pulling rate is adjusted by the heater power to be within the empirically-determined process window for dislocation-free growth, typically at or below 1 mm per minute. Solidification heat is conducted to the crystal surface and radiated to the chamber. For longer ingots the heat conduction is reduced and therefore the pulling rate has to be reduced. The crystal is rotated to homogenize the distribution of impurities and to suppress inhomogeneities in the temperature field. The crucible is rotated in the opposite sense to the crystal to stabilize the melt flow and control the oxygen concentration in the crystal.
The final stage of the crystal growth is the tail growth where the diameter is slowly decreased and a conical shape is achieved. The diameter of the solidification interface is reduced and dislocation formation is suppressed due to minimization of the thermal shock. Once the crystal has detached from the melt the power to the puller is decreased and the crystal is cooled down while being lifted into the upper chamber. At the end of the process, the crystal is removed from the puller for further processing.

2.2 Manufacturing of silicon wafers

Manufacturing of silicon wafers involves a series of mechanical, physical and chemical processes, all optimized to provide superior properties of the final wafer. A simplified manufacturing flow of the silicon wafer is shown in Fig. 2.
Wafer manufacturing follows the crystal growth process. First, the crystal crown and tail are cut off and the crystal body is divided into several pieces. Then the crystal quality (resistivity, oxygen and carbon content, dislocation-free state) is assessed on test wafers. Each section of the crystal is then surface-ground to the desired diameter, the crystal is oriented, and the flat is ground onto the cylindrical ingot. The flat identifies the orientation of the silicon wafers with respect to specific crystallographic directions; usually it corresponds to the (1 1;¯ 0) plane. Silicon wafers are sliced from the crystal sections using wire-saws or the inner-diameter (ID) saws. After edge grinding the wafer is lapped, etched and polished. Finally, the polished silicon wafer may have an epitaxial layer deposited on the prime surface by silicon epitaxy methods. Optionally the wafer backside can be coated

with a polysilicon layer and/or a protective layer of silicon oxide. After final cleaning and inspection the silicon wafers are suitable for device or integrated circuit (IC) manufacturing.

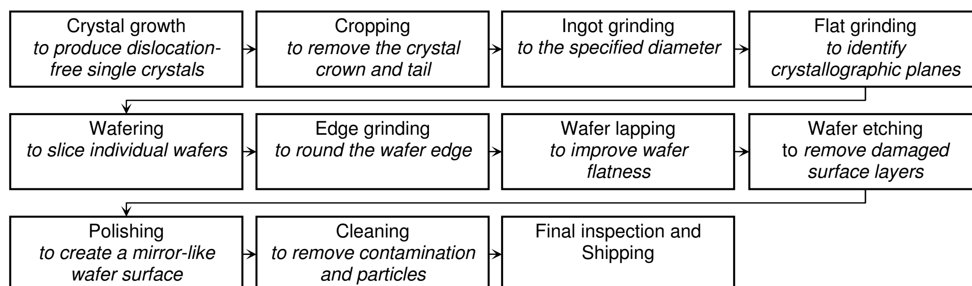

Fig. 2. Schematic manufacturing flow of the polished silicon wafer.

3. Defects in CZ silicon

Single crystalline CZ silicon wafer is a well-defined material of a very high quality. Nevertheless, it still may contain various defects which are formed either during the crystal growth or during processing of the silicon wafer. Defects which arise most frequently will be briefly introduced in the following sections. A detailed overview of defects in silicon can be found e.g. in (O´Mara, 1990).

3.1 Introduction

Soon after the start-up of mass production of dislocation-free silicon in the 1960’s it was realized that the highly pure silicon wafers suffered from enhanced formation of slip lines and degraded device yields as compared to formerly-used dislocated silicon. Later it was found that the issues were actually related to impurities and crystal defects.

Swirl-like distributions of agglomerates of silicon self-interstitials (so called A- and B-defects) were described first (Föll & Kolbesen, 1975), and vacancy agglomerates (so called C- and D- defects) were observed soon after (Roksnoer & van den Boom, 1981). Although the initial investigations were focused on FZ silicon, the defects were observed in CZ silicon as well, and obeyed essentially the same rules. The intensive research in the field revealed that formation of crystal defects depended on the crystal growth conditions. Several attempts were made to explain the occurrence of vacancy- and interstitial-type defects in silicon, but a unifying and generally accepted theory was not provided until the work of Voronkov (Voronkov, 1982).

The complete picture of defects in CZ silicon is even more complicated due to influence of impurity inherently tied to CZ silicon, namely oxygen. Oxygen preferentially occupies interstitial sites in the silicon lattice, but below about 1200°C it becomes supersaturated and tends to cluster and precipitate. Moderate oxygen precipitation significantly enhances the mechanical strength of the silicon wafer, whereas too strong precipitation can degrade the mechanical properties. Oxygen precipitates in the active region of an electronic device usually results in degradation of the device performance. On the other hand, oxygen precipitates outside of the active region may have a highly beneficial effect through intrinsic gettering (Rozgonyi, 1976). As there are both negative and positive effects closely related to oxygen precipitation, it is a phenomenon which has to be carefully engineered in the silicon

manufacturing technology. Oxygen precipitation depends on the concentration of interstitial oxygen, annealing conditions and oxygen interactions with intrinsic point defects. Hence, a lot of effort was directed to the investigation of defect formation in silicon during past decades.

3.2 Silicon crystal structure

Silicon crystallizes in the diamond cubic lattice (Bullis, 1991), which structure can be constructed as two interpenetrating face-centered cubic (fcc) lattices displaced along the unit cell body diagonal by the quarter of its length. The lattice constant of pure silicon is representing the length of the side of the fcc cube and has the value of 0.5431 nm at room temperature. Each silicon atom from one fcc lattice is covalently bound to its four nearest neighbors which belong to the other fcc lattice. In principle silicon wafer can be manufactured with the silicon lattice being oriented in any arrangement with respect to wafer surface. The common crystallographic orientations of wafer surface, described by Miller indices, are (100), (111) and (110). The crystal planes belonging to the families of these low-index crystal planes, i.e. {100}, {111} and {110} family, are the most important planes in the silicon lattice with the largest differences in various properties among these planes.

The closely spaced planes of the {100} family are the {400} planes with the interplanar distance of 0.1358 nm. The {220} planes with spacing of 0.1920 nm are the closely spaced planes of the {110} system. While spacing of all the {400} and {220} planes is equidistant, the situation is more complicated in case of the {111} system. The {111} planes of the fcc lattice are stacked in an ...ABCABC... manner, where none of the atoms in each layer is aligned with atoms in other layers when viewed perpendicularly to the stack. The {400} planes follow the ...ABCDABCD... scheme and the {220} planes follow the ...ABAB... scheme. Since the diamond lattice consists of two fcc lattices displaced along the direction perpendicular to the {111} system, stacking along <111> follows the ...AaBbCcAaBbCc... scheme. Here atoms in planes of the same letter overlap each other when viewed in <111> direction and capitalization distinguishes planes belonging to the two interpenetrating fcc lattices. The distance between adjacent planes of the same set (A-B, B-C and C-A) is 0.3135 nm; the distance between the closely spaced planes of the system a-B, b-C and c-A is 0.0784 nm and 0.2352 nm for the system A-a, B-b, C-c, which is the length of the covalent bond silicon-silicon. The closely spaced planes are bound strongly and often appear as one double plane. Different spacing of the crystal planes corresponds to different surface atom densities of 6.78×10^{14} cm^{-2} for {100} planes, 7.83×10^{14} cm^{-2} for {111} planes and 9.59×10^{14} cm^{-2} for {110} planes. The {111} plane shows the lowest surface energy and crystallizing silicon therefore tends to be bound by the {111} planes. Also the growth rate of the epitaxial layer is the lowest for the {111} oriented surface.

3.3 Classification and overview

Crystal defects are usually classified according to their shape and dimension. Silicon crystals and wafers may contain:

a. point defects- silicon self-interstitials, vacancies, interstitial impurities such as oxygen, substitutional impurities such as dopants and carbon,
b. line defects- edge and screw dislocations, dislocation loops,
c. planar defects- stacking faults,
d. bulk defects- agglomerates of point defects.

Some of the crystal defects are shown schematically in Fig. 3.

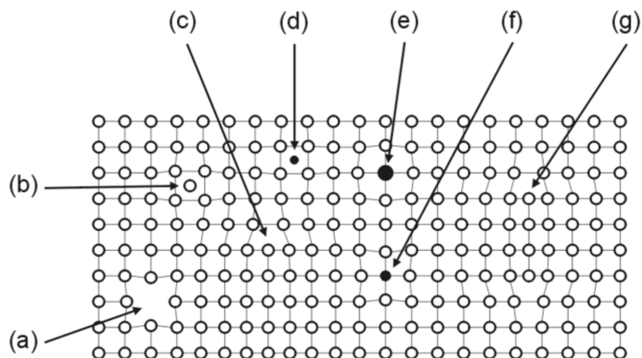

Fig. 3. Schematic 2D representation of crystal defects in silicon. (a) Vacancy, (b) self-interstitial atom, (c) edge dislocation, (d) interstitial impurity atom, (e) substitutional impurity atom of larger atomic radius, (f) substitutional impurity atom of smaller atomic radius, (g) extrinsic stacking fault.

3.4 Intrinsic point defects

Vacancies and silicon self-interstitials (Pichler, 2004) are intrinsic point defects inherent to the material whose occurrence in the lattice arises from thermodynamic equilibrium. Intrinsic point defects are incorporated into the growing crystal at the melt-crystal interface in their equilibrium concentrations. Point defects in the crystal are further created or annihilated by Shottky and Frenkel mechanisms, recombination, interaction with bulk defects, and injection during thermal wafer processing.

A silicon atom removed from its lattice site leaves behind four broken covalent bonds which can be arranged in several configurations. When the dangling bonds reform into molecular orbitals a neutral vacancy is formed. These orbitals are strained and can be relatively easily broken. Interaction with charge carriers results in formation of singly and doubly positively- or negatively-charged vacancies. The silicon self-interstitial is considered as an additional, more or less free atom occupying tetrahedral or hexagonal interstitial sites. Small clusters of vacancies and interstitials may be considered as a point defect. The precise atomic arrangement of vacancies and interstitials in silicon still remains somewhat uncertain, yet their effective thermodynamical properties such as concentration and diffusivity have been experimentally determined.

3.5 Extrinsic point defects

Dopant atoms are the primary extrinsic point defects in CZ silicon. The common dopant species - boron, arsenic, antimony and phosphorus - are introduced deliberately into the silicon melt during the crystal growth. They occupy substitutional sites in the crystal lattice and their concentrations are typically in the range of 10^{15} - 10^{19} cm^{-3}. The effect of dopant atoms on the properties of the crystalline silicon (besides the primary electric effect) originates from different atomic volumes, from interactions with intrinsic point defects, the formation of clusters, and from the effects on the diffusion and redistribution of impurities (Pichler, 2004).

Extremely undesirable point defects are *atoms of metallic elements* in the middle of the periodic table (Graff, 2000). Deep energy levels near the middle of the silicon forbidden band arising from metallic species act as effective generation-recombination centers and pose serious issues for device performance and process yield. The transition metals such as copper, nickel and iron are the most abundant contaminants. At high temperatures the metal atoms are usually distributed in the lattice occupying both interstitial and substitutional sites. As the temperature is reduced the metal atoms can form complexes with dopant atoms, and may eventually precipitate into bulk defects. The state of metals in the lattice depends on their solubility in silicon and on the imposed thermal cycles. The level of metallic contamination in semiconductor silicon for today's processes is typically below 10^{12} cm^{-3}. The steep decrease in solubility with decreasing temperature combined with a high diffusivity at low temperatures allows relaxation-type gettering techniques to remove the metals from the active device regions.

An unavoidable impurity in CZ silicon is *carbon* (O´Mara, 1990) introduced into the crystal growth system mainly from the graphite elements of the hot zone. Typical concentration of carbon in semiconductor silicon is below about 0.1 ppma ($5x10^{15}$ cm^{-3}). Carbon predominantly occupies substitutional sites in the silicon lattice. Due to its four valence electrons substitutional carbon is electrically inactive. Substitutional carbon forms complexes with oxygen. Interactions with silicon self-interstitials may lead to a displacement of the carbon into an interstitial position (Pichler, 2004). Interstitial carbon readily forms complexes with intrinsic point defects, substitutional carbon or dopants, which may become electrically active. Carbon was reported to promote oxygen precipitation. However, due to the low content of carbon in today's silicon, its the role in defect formation is of minor importance.

After dopant elements, *oxygen* is perhaps the most important extrinsic defect in silicon (O´Mara, 1990; Shimura, 1994). Oxygen is incorporated into the CZ silicon during the crystal growth. The silica crucible wall slowly dissolves into the silicon melt and oxygen is transported by diffusion and convection to the melt-crystal interface. Much of the oxygen evaporates from the melt free surface and only about 1% is incorporated into the growing crystal. The solubility of oxygen in silicon is a monotonically increasing function of temperature; its value at the melting temperature is about $2x10^{18}$ cm^{-3}. Oxygen concentration in the CZ silicon crystal is typically on the order of 10^{17} cm^{-3}. Oxygen atoms occupy interstitial positions in the silicon lattice where they are covalently bound to the two nearest silicon atoms. Interstitial oxygen may form electrically active chains known as “thermal donors”. Oxygen also forms complexes with intrinsic point defects (Pichler, 2004) which may play a role during the formation of bulk defects and promote oxygen diffusion.

3.6 Line defects

Today's CZ silicon crystals are grown in a dislocation-free mode (A-defects are not taken into account). Dislocations appear in silicon mainly due to stress generated by high temperature operations during the manufacturing of the wafer and devices on it when the critical resolved shear stress (CRSS) is exceeded. Edge and screw dislocations and dislocation loops are created under the high stress conditions, and have been observed in silicon mainly accompanying oxygen precipitates, self-interstitial agglomerates, dislocation arrays and tangles, and slip.

3.7 Planar defects

Two types of *stacking faults* (SFs) are generally distinguished, namely intrinsic and extrinsic faults. Intrinsic SF is formed by several missing atomic planes while the extrinsic SF is formed by excess atomic planes. SFs in silicon are always of the extrinsic nature (O´Mara, 1990) formed by discs of double planes inserted into the regular AaBbCc order of silicon {111} atomic planes. As the layers in the SF have to be added in pairs, one can drop the double index notation and describe the packing of the sequence with …ABCABC… In the SF region the order of planes is changed, such as …ABCACABC…. SFs are considered to be low-energy faults because they involve no change in the covalent bonds of the four nearest neighbors in the lattice (Hirth & Lothe, 1967). On the other hand, faults which disturb the nearest-neighbor covalent bonds are called high-energy faults (these are, for example, dislocations). The SF is bound by a Frank-type partial dislocation. A schematic drawing of such a SF is shown in Fig. 3. Other types of planar defects such as twin planes or grain boundaries are not present in properly-grown single crystal silicon.

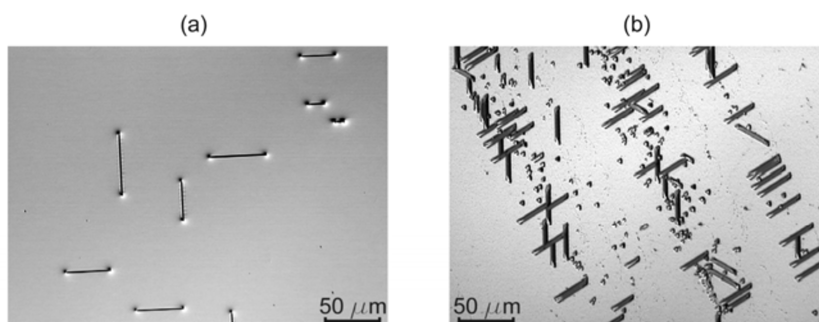

Fig. 4. (a) Bulk stacking faults on a (100) silicon surface. The varying SF length originates from the various depths of nucleation sites below the etched surface. (b) Surface stacking faults and dislocations on a (111) silicon surface. Predominantly equal SFs length confirms nucleation on the surface.

SFs originate from the condensation of silicon self-interstitials (Ravi & Varker, 1974), preferentially on suitable nucleation sites such as oxide precipitates, metal precipitates or mechanically damaged locations in the lattice. Surface and bulk SFs are distinguished according to the location of their nucleation site. Stacking faults can be delineated by selective etching of the sample surface and studied by optical microscopy or other inspection methods. The crystallographic origin determines the appearance of the SFs on the surface of silicon wafers of different orientations (see Fig. 4).
Bulk SFs in the silicon wafer may grow in the regions of strong oxygen precipitation (O´Mara, 1990), which is accompanied by a strong ejection of silicon self-interstitials. Growth of surface SFs can be also enhanced by an increased population of self-interstitials created by surface oxidation. SFs observed on the surface of polished silicon wafer after oxidation are referred to as "oxidation induced stacking faults" (OISFs).

3.8 Bulk defects

Vacancy-type defects. Supersaturated free vacancies present in the silicon crystal at high temperatures can agglomerate into voids (Itsumi, 2002). Voids (Fig. 5) take on an octahedral

shape bounded by {111} planes. The octahedral shape may be incomplete, truncated by {100} planes. Under favorable conditions, double- or triple-voids may appear. The inner void surface is covered by an oxide layer typically 2 - 4 nm thick. A typical void dimension is around 100 nm and a typical density in the crystal is about 10^6 cm^{-3}.

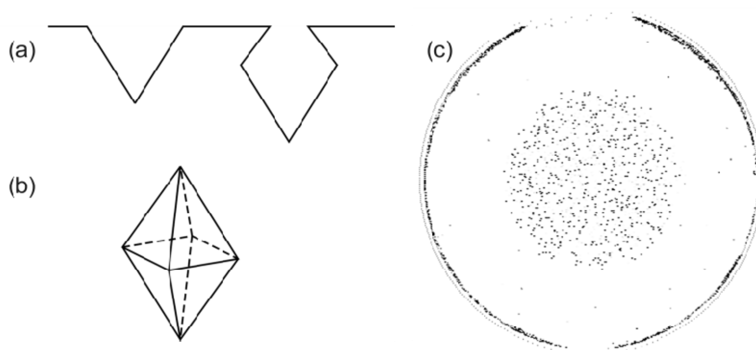

Fig. 5. Schematic representation of (a) COP defects on the wafer surface, and (b) a void defect in wafer bulk. (c) COP distribution observed by laser-type particle counter after dedicated SC1 treatment of the wafer with a vacancy-type core.

A void intersected by the wafer surface creates a pit referred to as the “crystal-originated particle” (COP) (Ryuta et al., 1990). The relation of a COP to a void is demonstrated in Fig. 5. The typical dimension of a COP does not allow direct observation on the polished wafer surface by common industrial equipment; a method such as atomic force microscopy (AFM) has to be used for the analyses. It was found that COPs can be observed after repetitive SC1 cleaning by commercial laser-type particle counters. COPs on the wafer surface can be delineated by other methods such as Secco etching where they appear as the wedge-shaped “flow pattern defects” (FPDs) (Yamagishi et al., 1992). Voids detected by infrared light scattering tomography are denoted as "LSTD" (Vanhellemont et al., 1997). Being vacancy agglomerates, COPs appear in the vacancy-type silicon (Fig. 5c).

Interstitial-type defects. Supersaturated silicon self-interstitials may coalesce into so called A- and B- defects (swirls). The B-defects are considered to be coherent globular clusters; the A-defects are large dislocation loops possibly formed by the collapse of the B-defects (Föll & Kolbesen, 1975). Large dislocation loops appear in size ranging from roughly a micrometer up to a few tens of micrometers with a density typically around 10^8 cm^{-3}.

Oxide precipitates. Due to the rapid decrease of oxygen solubility with temperature and the rather high oxygen concentrations in CZ silicon crystals, oxygen in silicon is usually present in a supersaturated state at most common process temperatures. The resulting precipitation of oxygen interstitials leads to the formation of oxide particles referred to as oxide precipitates or oxygen precipitates (Shimura, 1994). Oxide precipitates are formed of amorphous SiO_x, where x ranges from 1 to 2. Oxide precipitates of various morphologies have been observed: rod-like, square platelet, truncated octahedral, and polyhedral to spherical. The morphology of oxide precipitates depends on the formation conditions, mainly temperature and the degree of supersaturation. In principle it is determined by the stress energies associated with the precipitate growth (Borghesi et al., 1995). Growth of

oxide precipitates is usually accompanied by the formation of extended defects such as stacking faults and punched-out dislocation loops.

4. Impact of crystal defects on device yield

While the vacancy- and interstitial-type crystal defects have a detrimental effect on yield and the performance of electrical devices, oxide precipitates and associated extended defects can have both a positive and negative effect.

COP defects were shown to degrade gate oxide integrity (GOI) (Yamagishi et al., 1992) causing extrinsic dielectric breakdown of MOS capacitors and failures of the DRAM modules. Voids below the surface can result in excessive leakage currents in power devices. The gate oxide grown across a COP may be locally thinned or stressed on the COP edges where the electric field is locally greater; both these effects may lead to dielectric breakdowns, shifted device thresholds and leakage.

The presence of interstitial-type dislocation loops in the active regions of the devices may cause degradation of the minority carrier lifetime, alter diffusion profiles, and shift p-n junction characteristics (Abe et al., 1983). Due to their relatively large size they are especially harmful for today's processes characteristic by a high degree of device integration. The dislocations act as fast diffusion paths for impurities and dopant species. In particular, when decorated by metals, dislocation cores are sources of shorts and leakage currents.

Oxygen thermal donors can induce resistivity shifts in very lightly-doped silicon which affects numerous resistivity-dependent device parameters. The thermal donors are formed by rather weak binding energies and can be easily dissolved at temperatures above 600°C. As oxygen thermal donors are formed at a peak rate around 450°C the cooling rates during device manufacturing processes should be optimized in order to control the resistivity of the sensitive materials. On the other hand, the oxide precipitates are quite stable defects. Oxide precipitates in the active region of the device result in increased leakage currents in the p-n junctions, reduced refresh times in DRAM memories, reduced breakdown voltages in bipolar devices, degraded minority carrier generation/recombination lifetimes, and other serious failure mechanisms (see Schröder, 1989, and references therein). The root-causes of the failures are the precipitates themselves as well as the associated extended defects. On the other hand, oxide precipitates may have a positive effect through mechanical strengthening through impurity hardening (Sumino, 1980) and intrinsic gettering (Rozgonyi, 1976). However, oxygen precipitation has to be controlled in an optimal range for a given wafer processing flow, and a defect-free near surface region (so called “denuded zone”) should be guaranteed.

The effect of crystal defects on manufacturing processes and the properties of silicon wafers and electronic devices is quite varied and the impact is often fundamental. Hence, engineering of defects is inseparable across crystal growth and wafer processing. Due to the continuous evolution of silicon devices it is also a never-ending part of the technology of silicon crystal growth and wafer manufacturing.

5. Formation of grown-in defects in CZ silicon

In order to control formation of crystal defects in silicon wafers one has to understand the mechanisms of their formation from the very early stages of crystal growth. The basic mechanisms of defect formation during silicon crystal growth are described by the Voronkov theory (Voronkov, 1982) which will be briefly introduced in following sections.

5.1 Point defects - A pathway to crystal defects

Voronkov theory describes the formation of crystal defects consisting of several stages:

a. the incorporation of silicon self-interstitials and vacancies into the crystal,
b. transport, diffusion and recombination of the point defects,
c. nucleation and growth of defect clusters.

It is assumed that both silicon self-interstitials and vacancies are incorporated into the growing crystal at the melt-crystal interface. High diffusivities near the melting temperature and the proximity of the crystal surface acting as an effective source/sink allows the intrinsic point defects to exist in their equilibrium concentrations.

It is further assumed that the recombination rate of the point defects is high enough to maintain the product C_IC_V near its equilibrium value $C_I^{eq}C_V^{eq}$. As the equilibrium concentrations of the point defects decrease very rapidly with temperature, the $C_I^{eq}C_V^{eq}$ product quickly drops below the initial concentration of one of the point defects. This defect essentially vanishes and only the second specie survives. The type of the surviving defect is determined by the concentration of vacancies and interstitials prior to recombination, which is governed by the flux of the defects towards the region of effective recombination.

Vacancies and interstitials in the crystal diffuse by Fickian diffusion and thermodiffusion, and are drifted by the growing crystal. Voronkov assumed that the equilibrium concentrations of interstitials $C_I^{eq}(T_m)$, and vacancies $C_V^{eq}(T_m)$, at the melting temperature T_m are comparable, but $C_V^{eq}(T_m)$ is somewhat higher than $C_I^{eq}(T_m)$. Therefore, the drift flux of vacancies should be larger than that of interstitials. The drift (convection) is thus responsible for the supply of vacancies into the crystal, and the flux of vacancies into the crystal is proportional to the crystal growth rate, v. The diffusion flux is proportional to the concentration gradient which arises from the defect recombination processes. This, in turn, is determined by the axial temperature profile above the melt-crystal interface. The diffusion flux is therefore scaled in proportion with the temperature gradient, G. It is assumed that the diffusion coefficient of the self-interstitials is larger relative to that of vacancies. Hence, diffusion is responsible for the supply of interstitials into the crystal and the flux of interstitials into the crystal is proportional to the temperature gradient, G.

The concentration of the point defects above the melt-crystal interface is determined by the competition of the drift flux supplying vacancies and the diffusion flux supplying interstitials. As these fluxes are proportional to the crystal growth rate v, and to the temperature gradient G, respectively, the v/G ratio determines the type and concentration of point defects which survive the recombination stage. Point defect recombination proceeds at a significant rate around 1300°C. A typical temperature profile in the crystals grown in modern CZ crystal pullers results in a recombination length of about 2 - 3 cm from the melt-crystal interface. The v/G ratio in fact determines whether the silicon crystal a few centimeters above the melt-crystal interface (or at about 1300°C) contains vacancies or interstitials.

There is a critical value of the v/G parameter corresponding to the state when the drift and diffusion fluxes (or the vacancy and interstitial fluxes) are roughly balanced. In such a case the concentrations of vacancies and interstitials before the recombination are comparable and recombination leaves essentially defect-free crystal. The critical value of v/G, also referred to as ξ_t, is given by the point defects properties near the melting temperature. The critical ratio ξ_t separates two cases: (a) when the crystal growth process results in $v/G < \xi_t$, defect recombination results in a crystal populated by excess self-interstitials; or (b) when $v/G > \xi_t$, the crystal contains excess vacancies. The two cases are known as the interstitial-type crystal, and the vacancy-type crystal, respectively.

The surviving point defects become further supersaturated during cooling of the growing crystal which results in formation of bulk defects – vacancy-type defects in the vacancy-type crystal, and interstitial-type defects in the interstitial-type crystal. Also other phenomena such as oxygen precipitation may differ substantially between the vacancy-type and interstitial-type crystals. A silicon matrix rich in vacancies can easily absorb silicon interstitials emitted during the growth of oxide precipitates, while emission of interstitials into a matrix already rich in interstitials is energetically unfavorable. Oxygen precipitation in a vacancy-type silicon is generally stronger as compared to oxygen precipitation in an interstitial-type material. Taking into consideration the influence of crystal defects on wafer properties and device performance one realizes the importance of the crystal growth process, which determines the value of v/G.

5.2 Spatial distribution of defects

Principal distribution of defects in silicon crystal is determined by the relation of the v/G value to the critical value ξ_t. The crystal growth rate at a given crystal length can be considered constant across the melt-crystal interface from a macroscopic viewpoint. The temperature gradient, however, strongly varies across the radius. Due to cooling of the crystal surface by radiation and convective heat loss to the atmosphere the axial temperature gradient at the melt-crystal interface increases from the crystal center to the perimeter. The v/G parameter thus decreases from the center to the perimeter (see Fig. 6). The relation of the ξ_t value to the v/G curve determines whether an interstitial-type, a vacancy-type, or a mixed-type crystal is grown, as illustrated in Fig. 6. The transition between the vacancy-type and interstitial-type portion of the crystal is called the vacancy–interstitial boundary (V-I boundary). As the process conditions vary during the crystal growth, the v/G curve changes also with the crystal length.

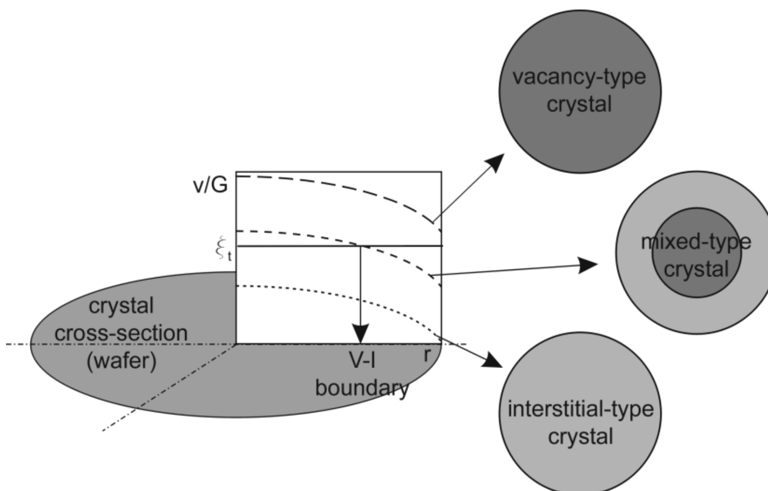

Fig. 6. Left: a typical radial dependence of the v/G ratio and three possible relations of the $v/G(r)$ curve to the critical parameter ξ_t. Right: crystal (wafer) types determined by the relation of $v/G(r)$ to ξ_t. The cross-section image corresponds to a wafer sliced from the crystal.

As noted above, formation of bulk defects in silicon is strongly influenced by the type of the material. The nature of the crystal from the defect point of view (distribution of the vacancy-type and interstitial-type regions) in principle determines the presence and distribution of bulk defects in the silicon wafers. Today's FZ silicon crystals are typically of fully vacancy-type due to high growth rate which is typically 2 - 3 times higher compared to CZ silicon crystals. On the other hand, CZ silicon crystals of all three types shown in Fig. 6 can be found. First CZ silicon crystals were of the interstitial-type, due to a relatively high value of *G* in the crystals of small diameter. Today's 6" and 8" crystals produced at a rather high pull rates are usually of vacancy-type. The 300 mm crystals may be of the mixed-type and even larger crystals may become fully interstitial-type because of the pull rate which has to be decreased when increasing the crystal diameter up to these levels (von Ammon et al., 1999). Doping elements and their concentration in the crystal can significantly influence formation of crystal defects and shift the process in favor of either vacancy-type or interstitial-type (Borionetti et al., 2002).

5.3 Oxygen precipitation

Oxygen precipitation, i.e., the formation and growth of oxide precipitates from the supersaturated solid solution of oxygen in silicon can be characterized as a two-step process consisting of a nucleation stage and a growth stage. A comprehensive introduction on oxygen precipitation theory can be found in (Shimura, 1994; Borghesi, 1995).
Nucleation is the process of formation of aggregates of a small number of oxygen atoms - the nuclei (or precipitate embryos). Due to relatively low annealing temperatures the supersaturation is high but the diffusivity of oxygen is low. The change in the concentration of interstitial oxygen in the silicon matrix is usually negligible and mainly the precipitate density is established. Precipitate growth (often referred to as the precipitation stage) is caused by diffusion of oxygen atoms and attachment to the existing nuclei at higher temperatures. While the generation of new nuclei during the precipitation stage is negligible the existing nuclei grow substantially while forming oxide particles of sizes reaching up to the micrometer scale. The supersaturation in this stage is lower but the diffusivity of oxygen is much higher than in the nucleation step. During precipitation the reduction in the concentration of interstitial oxygen may be dramatic.

Annealing Step		Precipitated oxygen [%]
750°C/10h	-	1.0 ± 0.5
750°C/40h	-	46 ± 3
750°C/10h	1050°C/20h	91.4 ± 0.5

Table 1. Influence of annealing temperature and time on the amount of precipitated oxygen in a lightly boron doped wafer with an interstitial oxygen content of 9.7×10^{17} cm^{-3}.

The influence of various annealing steps on the reduction of interstitial oxygen is shown in Table 1. Although shorter annealing at low temperature (750°C/10h) reduces the interstitial oxygen concentration only by about 1%, the nuclei have sufficient size for further growth during a precipitation step at 1050°C. It is also shown that even low temperature annealing can reduce interstitial oxygen significantly if the annealing time is extremely long and the initial interstitial oxygen concentration is sufficiently high.
Capturing the nucleation stage has been the most difficult problem over the decades of oxygen precipitation studies. The precipitate nuclei are too small to be observed directly

therefore only indirect observations have been used for model validations. Further complications resulted from the uncertainties in the thermo-physical properties of the various defects involved in the nucleation phase. The topic has been treated by numerous authors who assumed both homogeneous and heterogeneous nucleation mechanisms (e.g., Borghesi, 1995, and references therein). Regardless of the particular nucleation mechanism there is a parameter crucial for all theoretical considerations – the critical radius of the nucleus which determines the temperature stability of the nucleus. Nuclei of radius smaller than the critical radius corresponding to the actual temperature tend to dissolve while the larger ones continue to grow.

In order to overcome the lack of analytical methods for identifying the nucleation stage the experimental studies often use various thermal treatments for growing the oxide precipitates to a detectable size and deducing the nucleation processes from the precipitation behavior. The early work resulted in the establishment of procedures for optimization of oxygen precipitation, e.g. for intrinsic gettering. Classical precipitation treatment of silicon wafer consists of a low temperature nucleation step (~700°C) followed by a high temperature precipitation step (~1000°C).

While the nucleation stage of oxygen precipitation remained rather mysterious, the growth of oxide precipitates became experimentally well-described. As shown by many authors oxide precipitates formed during wafer thermal treatments usually show the diffusion-limited growth according to the theory of Ham (Ham, 1958). The precipitate growth controlled by oxygen diffusion results in a square-root dependence of the precipitate size on annealing time at a given temperature. However, due to several assumptions, Ham's theory is not always applicable. The early works usually considered silicon wafer as "clean" input material. However, it has been gradually recognized that some nuclei are formed already during the silicon crystal growth process, and the importance of the thermal history and intrinsic point defects has been recognized.

State-of-the-art investigations of defect formation in silicon thus start from the early beginnings of the crystal growth process, and the interplay of all intrinsic and extrinsic point defects present in the crystal must be considered.

5.4 OISF ring

An interesting feature related to oxygen precipitation during crystal growth is observed on silicon wafers of the mixed-type after oxidation of the surface. Rapid oxidation of the wafer surface (wet oxidation) results in the injection of silicon interstitials below the oxidized surface. These interstitials can condense into stacking faults on grown-in oxide precipitates in the near-surface region. A ring of relatively large oxygen precipitates can be formed near the vacancy-interstitial boundary during the crystal growth process (Voronkov, 2008). This phenomenon results in a ring-like distribution of stacking faults (Hasebe et al., 1989) during subsequent wet oxidations. The observed feature (see Fig. 7) is referred to as the "oxidation-induced stacking fault ring" (OISF ring).

The OISF ring can be easily visualized on an oxidized wafer by stripping the oxide and selectively etching the surface. The etched OISFs are visible by optical microscopy and the OISF ring is detectable even by the naked eye. The OISF ring is located on the edge of the vacancy-type core in mixed-type crystals close to the V-I boundary. Due to the ease of detection it has been widely used for delineating the V-I boundary and investigating the defect distribution in silicon crystals.

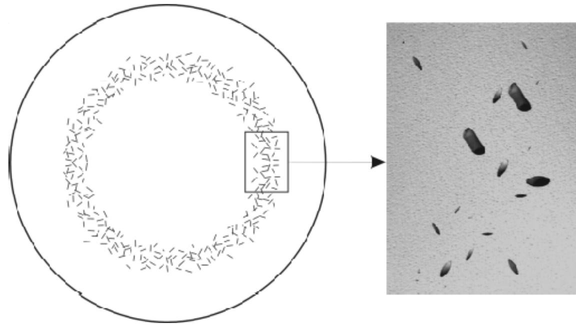

Fig. 7. OISF ring on the surface of a silicon wafer.

6. Methods of studying crystal defects

In order to capture the distinctive nature of crystal defects and the wide range of their size and density, various methods are used for defect analyses. The most common techniques are briefly introduced in following section.

6.1 Preferential etching

Analytical methods based on preferential etching of silicon are frequently used for studying defects in silicon technology. All modern defect etchants for silicon are based on the chemistry of formation and dissolution of silicon dioxide, and therefore all etchants include hydrofluoric acid. The dissolution process is enhanced at and around defects due to weakened bonds and coalescence of impurities around them. The electronic properties may play a role, too. Etching anisotropy with respect to various crystallographic planes (atom density) also has to be taken into account. In general, the etch rate is lowest for the {111} crystal planes. The most common etching solutions are those of Wright, Sirtl, Schimmel, Yang, Secco, MEMC, and Dash. Individual solutions are optimized for various surface orientations, conductivity types or resistivity levels. For more details on use and application see (ASTM standard F 1809–02, 2003).

Preferential etching allows for rather simple detection of dislocations, stacking faults, slip lines, and oxide precipitates as shown in Fig. 8. Individual defects on the etched surface may be observed by optical microscopy or SEM, while defect distributions across a wafer can be observed by the naked eye in most cases.

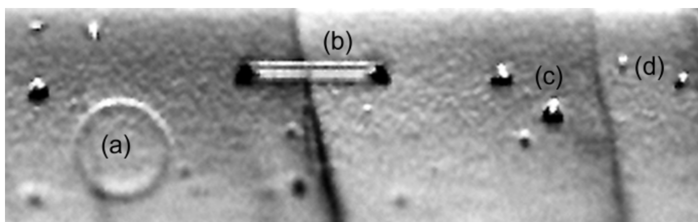

Fig. 8. Defects in silicon revealed by preferential etching of a cleaved surface. (a) A stacking fault in the cleavage plane, (b) a stacking fault tilted with respect to the cleavage plane (note the bounding dislocation), (c) dislocations, (d) oxide precipitates.

6.2 X-ray topography

X-ray topography (Lang, 1978) is based on Bragg diffraction. A monochromatic X-ray beam incident on a surface is reflected by the atomic planes of the crystalline sample. Constructive interference occurs when the Bragg condition is fulfilled. The diffraction pattern is recorded on the detector either in reflection geometry (Bragg geometry) or transmission geometry (Laue geometry).

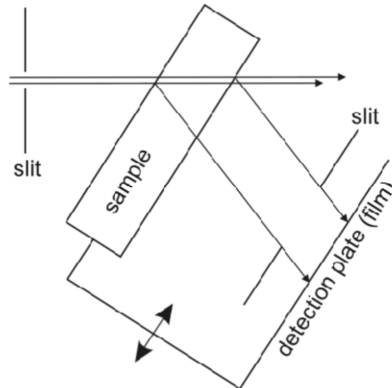

Fig. 9. Schematic layout of the X-ray section and projection topography in Laue geometry.

In the case of section topography, a very narrow beam of dimensions in the order of 10 µm is used. The section topographs therefore investigate only a small volume (section) of the sample. The beam is diffracted at different depths, each one contributing to the image on a different location on the detector. Section topography is therefore used for depth-resolved defect analysis. When the sample and detector are simultaneously moved with respect to the incident beam, the sample is scanned over a larger volume and a projection topograph is formed. The schematic configuration of X-ray topography in Laue geometry is shown in Fig. 9. A homogeneous crystal lattice generally results in a homogeneous distribution of intensity across the topograph. Section topography, however, results in spatial variations in the intensity of diffracted rays even in a perfect crystal (so called Pendelösung fringes) due to the dynamic nature of diffraction and a small investigated volume. Irregularities of the crystal lattice, such as defects and strain, are captured as a distortion of the image of the perfect crystal. X-ray topography can detect irregularities such as phase boundaries, defective areas, cracks, scratches, growth striations, and most of the common crystal defects such as dislocations, oxide precipitates, stacking faults, and interstitial-type defects. An example of X-ray topography results is shown in Fig. 16.

6.3 Fourier transform infrared spectroscopy

Fourier transform infrared spectroscopy (FTIR) is the most common technique for determining the concentration of oxygen in silicon materials. The polychromatic source radiates infrared (IR) light through a Michelson interferometer. The radiation is transmitted through the silicon wafer and directed to a detector. Undoped silicon is transparent to the IR radiation. Impurities cause localized absorption from lattice vibrations. The absorption due to the anti-symmetric vibrational mode at 1107 cm^{-1} has been assigned to interstitial oxygen

and it is thus used for determining the oxygen concentration. In order to suppress the influence of the silicon lattice vibrations and to allow the quantitative analysis, a reference spectrum is subtracted from the measured spectrum. The reference spectrum is measured on float-zone silicon prepared with very low oxygen content (less than 1×10^{16} cm^{-3}). After signal processing and taking the wafer thickness into account, the intensity of the oxygen absorption peak is calculated, and thus, the concentration of oxygen may be determined as the product of the peak intensity and a tabulated conversion factor. The selected conversion factor has to be reported together with the concentration value. The oxygen concentrations presented in this work are given in accordance with the ASTM standard (ASTM Standard F1188-02, 2003) commonly referred to as "new ASTM". The FTIR method is not applicable for heavily-doped silicon as this material is not transparent to IR radiation due to the high concentration of free carriers.

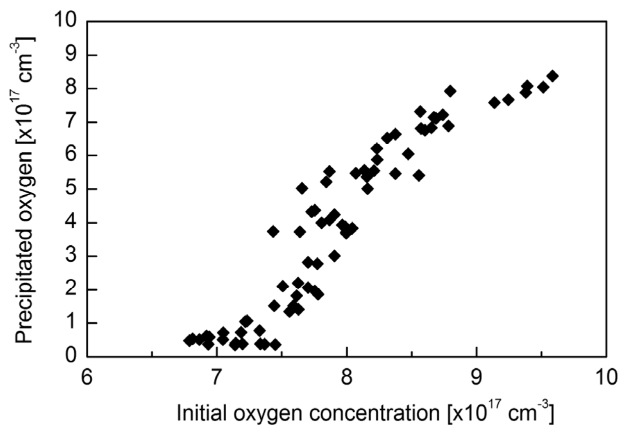

Fig. 10. An example of an “S-curve” characterizing oxygen precipitation in the crystal grown by a particular crystal growth process.

As the contribution of precipitated oxygen atoms to the absorption peak of interstitial oxygen is small (absorption energies are shifted), the FTIR measurements of interstitial oxygen concentration can be used for characterization of oxygen precipitation. The difference in the content of interstitial oxygen prior to, and after, the heat treatment is the measure of oxygen precipitation, relevant for the specific sample material and thermal cycles. For overall characterization of a crystal grown by a particular growth process the dependence of the precipitated oxygen on the initial oxygen concentration is constructed for a standardized thermal cycle. The dependence is called the "S-curve" because of its typical sigmoidal shape (Fig. 10). Another application of the S-curves is the comparison of different thermal cycles (e.g., in IC production) with respect to oxygen precipitation.

6.4 Precipitation test

This test is aimed at assessing the precipitation behavior in the wafers. Oxide precipitates formed in the crystal during growth (grown-in precipitates) are usually too small to be detected directly as noted previously. Oxygen precipitation is therefore evaluated in silicon wafers subjected to a standardized thermal treatment sequence.

Generally, two types of the heat treatment are used: (a) single step annealing at high temperature when the grown-in oxide precipitates are allowed to grow, and (b) two-step annealing which includes also a low-temperature nucleation step. Typical thermal cycles for such heat treatments are the 1050°C/16h annealing, and 750°C/4h + 1050°C/16h annealing. The extent of oxygen precipitation is evaluated as the difference in oxygen concentration before, and after, the thermal treatment as measured by FTIR, or by “cleave-and-etch” analyses. In such cases, the wafer cross-section is prepared by cleaving or grinding, the sample is preferentially etched, and the defect distribution and density is evaluated under the microscope. An example of the cleave-and-etch analysis is shown in Fig. 11.

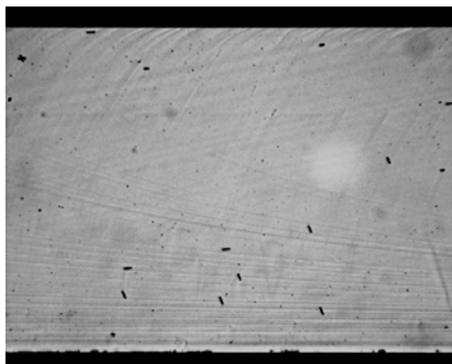

Fig. 11. A wafer cross-section prepared by the cleave-and-etch method. The wafer front surface (polished) is at the top of the figure. The analysis reveals oxide precipitates (dots) and stacking faults (short lines) in the bulk of the wafer.

6.5 OISF test

The OISF test uses the fact that silicon interstitials injected below the wafer surface during oxidation under usual conditions needs a suitable nucleation site for formation of OISFs (Ravi & Varker, 1974). The test wafer is subjected to an oxidation cycle (e.g., 1000°C/1hr in a “wet” atmosphere), then the grown oxide is stripped with HF acid and the surface is preferentially etched. The stacking faults observed on the surface decorate the nucleation centers in the near-surface wafer region. The nucleation sites can arise from the sub-surface damage caused by the wafer manufacturing processes, handling, etc., from wafer contamination, and defects such as dislocations and oxygen precipitates. The OISF test is therefore used as a general method for assessing the quality of the wafer surface. If the manufacturing process is optimized and wafer contamination is avoided, the OISF test can be used for delineation of crystal defects in the wafer as in the case of the OISF ring.

6.6 COP test

Delineation of COPs is based on SC1 cleaning and "particle" inspection methods (Ryuta et al., 1990). As the typical COP dimensions do not allow direct observation on the polished wafer surface by common industrial equipment, the SC1 cleaning chemistry is used to etch the COPs and enlarge them to dimensions greater than the detection limit of the instruments. The size of COP defects after the SC1 treatment is typically 100 - 300 nm and the surface density is of the order of 10 to 100 cm^{-2}. An example of the measurement output is shown in Fig. 5c.

7. Engineering of crystal defects in silicon

Defect engineering in production manufacture of silicon wafers comprises modifications of the crystal growth process and dedicated heat treatment of the wafers. The primary objective is usually the control of oxygen precipitation and the associated defect structures. The specific requirements on the spatial distribution, size and density of oxide precipitates may differ for various devices, but the basic features are essentially the same. It is desirable to achieve a defect-free region near the surface of the wafer so that the devices fabricated there do not suffer from the electrical effects resulting from the presence of the defects. On the other hand, a high density of oxide precipitates is usually required in the bulk of the wafer in order to provide effective intrinsic gettering. The near-surface region free of oxide precipitates is called a "denuded zone".

7.1 Denuding and precipitation of oxygen

The classical procedure for forming the desired denuded zone and achieving intrinsic gettering utilizes a three-step thermal treatment (Nasagawa et al., 1980) demonstrated in Fig. 12a. The first step is the denudation at high-temperature which results in dissolution of the grown-in oxide precipitates and subsequent out-diffusion of oxygen from the wafer surface. Oxygen diffusivity above 1100°C is sufficiently high to result in a depleted zone of several tens of micrometers depth, while the oxygen concentration in the bulk far from the wafer surface retains its initial value. The shape of the transition from the solubility limit value at the surface to the bulk value is determined by the annealing time (Fig. 12b, $C_0 = 8\times10^{17}$ cm^{-3}).
The second step causes the nucleation of new oxide precipitates at temperatures around 700°C. During the third step, called the precipitation stage, nucleated oxide precipitates grow in the regions of sufficiently high oxygen concentration, while no oxide precipitates grow in the depleted region near the surface and the denuded zone is formed. The experimentally observed limit of oxygen concentration necessary for appreciable precipitation is around 6.6 - 7 $\times10^{17}$ cm^{-3} (see Fig. 12b) and varies depending on the type and concentration of dopant species.

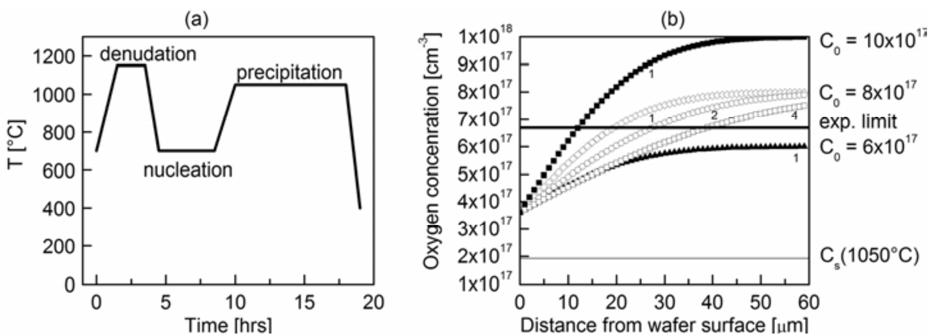

Fig. 12. (a) An example of a thermal cycle for formation of the denuded zone and effective intrinsic gettering. (b) The concentration of oxygen in the wafer with initial oxygen concentration C_0 denuded at 1150°C. Denuding duration in hours is noted in the plot below the curves. The thin horizontal line in (b) represents the equilibrium concentration of oxygen at the temperature of the precipitation step (1050°C); the thick solid line represents the experimental limit of oxygen precipitation. Out-diffusion profiles in panel (b) were calculated after (Andrews, 1983).

The depth profile of the precipitated oxygen in the silicon wafer can be calculated on the basis of the interstitial oxygen depth profile (Borghesi et al., 1995). As shown in Fig. 12b, the oxygen concentration after out-diffusion provides certain supersaturation even in the denuded zone, but the amount of precipitated oxygen depends more strongly on the density of nuclei than on the level of oxygen supersaturation during precipitation. This latter point is critical in making material stable to large thermal budget wafer processing. The nucleation rate during the second step is very strongly reduced for low oxygen concentrations in denuded zone, e.g., the rate was reduced by more than ten times for oxygen concentration reduced by 2×10^{17} cm^{-3} (Borghesi et al., 1995). As a result the region near the surface is precipitate-free and the bulk region is precipitate-rich. The transition between the bulk and the surface is not sharp; it follows the initial oxygen profile (see the dependence in Fig. 14 below).

7.2 Wafer annealing

It was found that high temperature annealing can help control and manage also other types of crystal defects, not simply oxide precipitates. The COP defects on the wafer surface can be annihilated during high temperature annealing in hydrogen (Nadahara et al., 1997), or in argon ambient (Adachi et al., 1998). As shown in Fig. 13, proper treatment of the polished wafer can significantly reduce or even eliminate COP defects on the surface of polished silicon wafers. However, attention has to be paid to oxygen precipitation in the bulk of the wafer, since during the high temperature annealing applied for annihilation of COPs the grown-in oxide precipitates tend to dissolve. Subsequent oxygen precipitation in the annealed wafer may become suppressed and the wafer can loose its gettering capability.

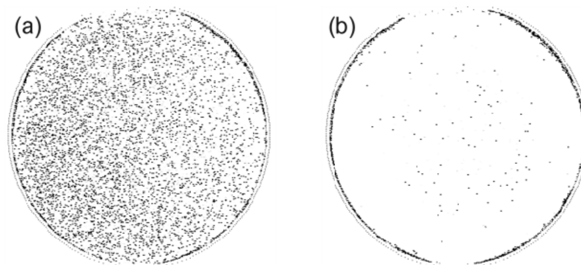

Fig. 13. COP distributions measured by a particle detector (lower dimensional detection limit is 0.13 μm) on vacancy-type wafers (a) before and (b) after hydrogen annealing (1180°C/2hr).

7.3 Optimization of oxygen concentration in the crystal

The denuded zone and intrinsic gettering are closely related to oxygen precipitation, which in turn strongly depends on the oxygen concentration in the wafer. Fig. 12 demonstrates the thickness of the denuded zone, and Fig. 14 shows the density of oxide precipitates, both as the function of oxygen concentration. As the oxygen concentration in silicon is determined during the crystal growth process, control of the oxygen concentration in the growing crystal is one of the primary tasks for crystal growers.

As was previously discussed, oxygen is incorporated into the crystal at the melt-crystal interface, while its concentration in the crystal relates to concentration in the melt. The

concentration of oxygen in the melt below the crystal is determined by the source (crucible materials), by the effectiveness of the transport in the melt, and by the strength of the sink, i.e., by the dissolution rate of the silica crucible, by the melt flow, and by the evaporation from the melt surface. Critical process parameters driving these phenomena are the hot zone design, the crucible rotation rate, and gas atmosphere parameters. All of the parameters are usually optimized to reach a desired oxygen concentration in the whole crystal with limited variation and good reproducibility. Typical concentrations of oxygen in CZ silicon crystals range from about 11×10^{17} cm^{-3} down to about 6×10^{17} cm^{-3}; special designs of the hot zone (usually utilizing shields for gas flow control) allow decreasing oxygen concentration slightly below 5×10^{17} cm^{-3}.

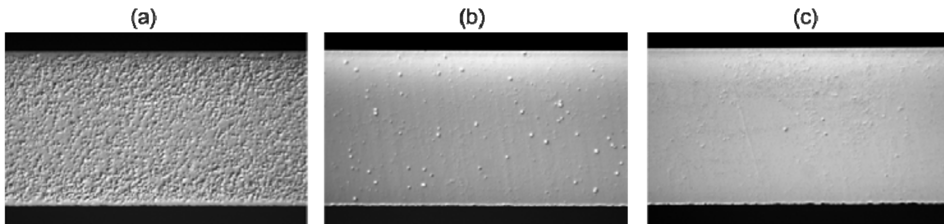

Fig. 14. Oxide precipitates delineated by preferential etching after 750°C/4hr + 1050°C/16hr annealing in lightly phosphorus-doped silicon wafers with oxygen content of (a) 8×10^{17} cm^{-3}, (b) 7×10^{17} cm^{-3}, (c) 6×10^{17} cm^{-3}.

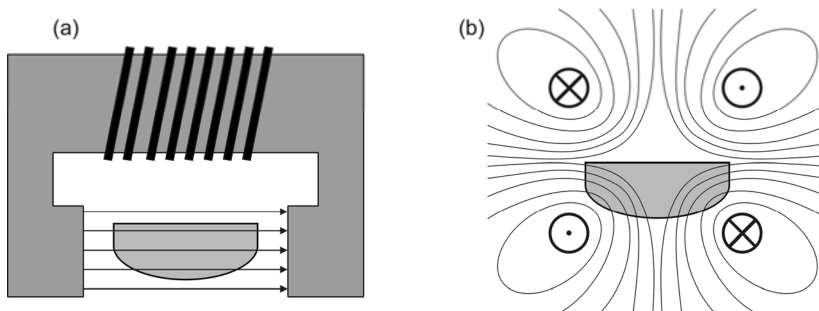

Fig. 15. Schematic drawing of (a) transverse and (b) cusp magnetic fields for control of the melt convection during crystal growth.

There are applications which require extremely low oxygen concentrations or very uniform distributions of oxygen in the crystal. These requirements are beyond the capability of most standard Czochralski crystal growth processes. Magnetic Czochralski process (MCZ) has to be used to achieve reduced concentrations of oxygen in the silicon crystals. The principal aspect of MCZ lies in the influence of the Lorentz force on the convection in the melt, which arises from the interaction of magnetic field with the fluid flow of the highly electrically conductive silicon melt. The effect of various kinds of magnetic fields has been studied extensively (Hurle, 1993). Based on many investigations, only transverse (horizontal) and cusp magnetic fields are used in industrial applications. The two configurations are schematically shown in Fig. 15. The horizontal magnetic field is used for growth of large

diameter crystals, while for smaller diameter crystals the cusp field is applied. The two most important effects of the magnetic field generally consist in damping of micro-scale growth rate instabilities at the melt-crystal interface through damping of melt temperature fluctuations, and in the possibility of tuning the incorporation of impurities into the growing crystal. Application of the magnetic field adds additional degrees of freedom to the crystal growth process which widens the capability of the process, but simultaneously brings complexity related to the higher technological level of the process.

7.4 Nitrogen doping

Extremely low oxygen concentration allows for the formation of very deep denuded zones, but also results in negligible oxygen precipitation in the bulk. Oxygen precipitation is generally low also in heavily-doped n-type wafers due to enhanced evaporation of dopant atoms in the form of oxides. For applications requiring effective intrinsic gettering this drawback can be solved by nitrogen doping. Introducing nitrogen in silicon crystal results in enhanced precipitation of oxygen during subsequent wafer annealing due to stable nuclei formed during the crystal growth, an increased concentration of free vacancies available for oxygen precipitation and consumption of the interstitials emitted during the precipitate growth (von Ammon et al., 2001). Effective intrinsic gettering then can be achieved even at low oxygen concentrations or under conditions of unfavorable thermal treatments, such as argon or hydrogen annealing (Ikari et al.). The effect of nitrogen doping on oxygen precipitation is demonstrated in Fig. 16.

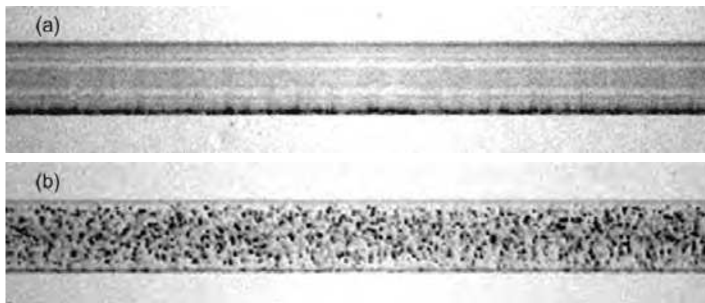

Fig. 16. An X-ray section topograph showing the effect of nitrogen doping on oxygen precipitation in heavily antimony-doped wafers with low oxygen concentration. (a) Standard wafer. (b) A wafer co-doped with nitrogen at the level of 5×10^{14} cm^{-3}. Wafer (a) is "defect-free". The horizontal Pendelösung fringes are clearly visible (see Section 6.2). Strain related to the polysilicon layer on the wafer backside (bottom) results in dark features in the topograph. A section topograph of wafer (b) shows oxide precipitates (dark spots) and residual damage on the wafer backside (bottom). The wafer thickness is 625 μm.

7.5 Vacancy-controlled denuded zone

An elegant solution to overcome the dependence of denuded zone parameters on the oxygen concentration was developed by Falster et al. (Falster et al., 1998). The concept of so-called "Magic Denuded Zone" (MDZ) utilizes the importance of vacancies for oxygen precipitation. The concentration profile of vacancies in the wafer is modified via rapid

thermal annealing (RTA). Annealing at temperatures of about 1200°C forms a population of vacancies and interstitials in equal concentrations through the generation of Frenkel pairs. Point defects reach their equilibrium concentrations in a short period (a few tens of seconds) throughout the thickness of the thin wafer by diffusion to and from the surface. During cooling of the wafer to low temperatures, the equilibrium concentrations of point defects decreases, providing a driving force for enhanced diffusion and recombination. This favors diffusion to the surface, where equilibrium is maintained. However, when the cooling rate is fast enough, the diffusion is effective only in the near-surface region. In the bulk of the wafer, only point defect recombination takes place leaving behind a population of excess vacancies at a concentration given by $C_v^{eq}(T_a) - C_i^{eq}(T_a)$, where T_a is the annealing temperature. The MDZ wafer finally contains an essentially vacancy-free surface and a transition region below the surface with steadily increasing vacancy concentrations up to the bulk level.

When an MDZ wafer passes through a high temperature anneal oxide precipitates nucleate and grow only in the region with sufficient vacancy concentrations which results in the denuded zone at the wafer surface. The depth of the Magic Denuded Zone can reach even deeper into the bulk than the classical denuded zone, but the solution has another major advantage– the result is practically independent of oxygen concentration in the wafer. Although the MDZ comprises an extra treatment of the wafer it suppresses the need for complicated oxygen control in CZ silicon crystals.

7.6 Optimization of v/G

Sometimes annealing of the wafer cannot meet the requirements of the wafer processing thermal budget. In such cases, formation of defects in the wafer can be adjusted by controlling the distribution of point defects in the growing crystal. As described above, vacancy-type or interstitial-type regions are formed in the crystal depending on the v/G parameter. The different regions within the crystal contain different types of defects and also substantially differ in oxygen precipitation characteristics. Tuning of the crystal growth rate v, and/or the temperature gradient G, can shift the V-I boundary and so influence defect formation.

There are often issues with excessive oxygen precipitation in heavily-boron doped wafers which results in electronic devices with excessive leakage currents. Analyses showed that the strong precipitation is constrained within the vacancy-type region in the portion of the crystal with the highest oxygen concentration (Valek et al., 2007, 2008). If the oxygen profile of the particular crystal growth process cannot be altered, then the crystal growth rate may be optimized to eliminate the vacancy-type region from the crystal (Fig. 17). The low growth rate shifts the v/G curve below the critical value ξ_t (see Fig. 6), the material becomes interstitial-type in full cross-section and oxygen precipitation is suppressed.

7.7 Computer simulations of crystal growth

Distribution of crystal defects in silicon wafers is significantly predetermined by the formation of defects during the crystal growth. Incorporation of point defects into the crystal and formation of crystal defects are driven by the time evolution of the temperature field, which governs the solubility and the diffusivity of the various species. However, measurement of the temperature field (necessary for its control) in the growing crystal is practically impossible. The analysis of grown-in defects after the crystal growth is very

difficult due to their small size which is often below the detection limit of common techniques. Therefore, detailed numerical models have been developed to overcome these obstacles by computer simulations which help to describe and predict defect formation from the crystal growth up to the point of wafer processing and device manufacturing (Brown et al., 2001; Dupret & Van den Bogaert, 1994; Kalaev et al., 2003).

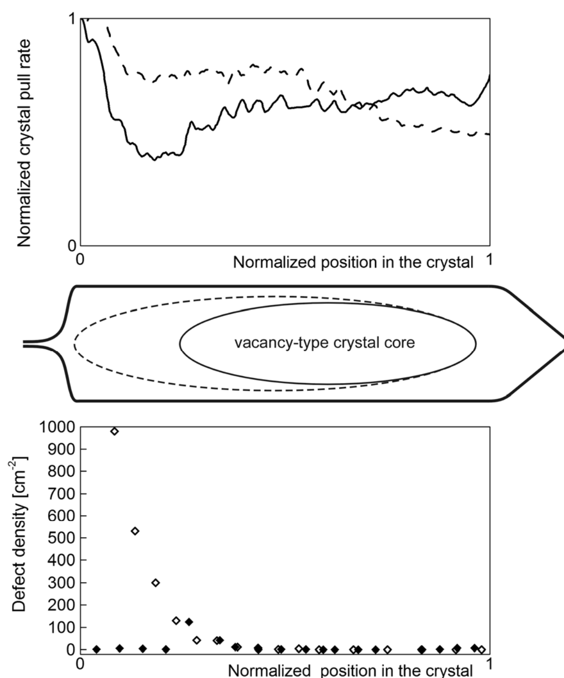

Fig. 17. An example of defect engineering through *v/G* control. The axial profile of the crystal pull rate (top), the distribution of point defects (middle), and the corresponding defect density (bottom) of the original (dashed lines, open symbols) and optimized (solid lines, solid symbols) crystal growth process.

Simulations of *v/G* are the simplest method for prediction of defect formation in the crystal. Comparing the simulated *v/G* values with the critical *v/G* value allows the identification of the vacancy-type and interstitial-type regions of the crystal separated by the vacancy-interstitial boundary. For example, a complicated distribution of OISFs on the oxidized surface of heavily boron-doped wafers was identified (Valek et al., 2007, 2008). The OISFs formed a pattern of two concentric rings (radii R_1 and R_2 in Fig. 18) on wafers from the beginning of the crystal. With increasing distance from the seed end of the crystal the OISF density decreased and the rings gradually disappeared.
In order to identify origin of the rings the temperature gradient, *G*, at the melt-crystal interface was modeled at several positions in the crystal using FEMAG code (Dupret & Van den Bogaert, 1994) and the corresponding radial *v/G* curves were calculated. Using the ξ_t values the V-I boundary was constructed. In Fig. 18 the V-I boundary was found to go through the whole crystal. It was concluded that also the OISF pattern should be formed

throughout the whole crystal. This conclusion was supported by a special OISF test with pre-annealing of the wafers. This annealing was performed to enlarge the grown-in oxide precipitates to a supercritical size for the OISF test. Finally, the origin of the “strange” OISF pattern was explained in terms of oxygen concentration and thermal history, see (Valek et al., 2007, 2008), for more details. This work demonstrated the value of computer simulations of crystal growth as a necessary tool for defect engineering.

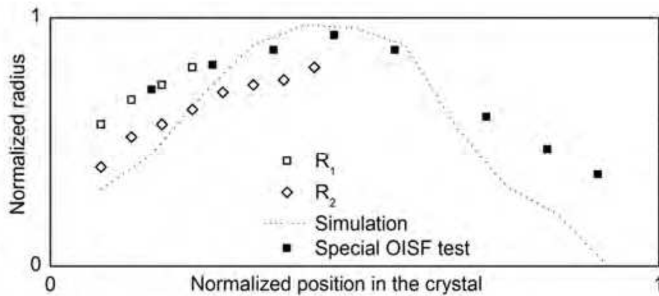

Fig. 18. Plot of the radius of the rings forming the OISF pattern, the simulated V-I boundary, and the radius of the OISF pattern delineated by a special OISF test (with pre-annealing).

8. Conclusion

Crystal defects are formed in silicon during the growth of the single crystals and processing of the wafers. Depending on their nature, density and size, these defects may substantially influence silicon material properties and consequently strongly impact process of device manufacturing. We provided the reader with a brief outlook of crystal defects in silicon and introduced the mechanisms of their formation. Knowledge of these mechanisms is the fundamental requirement for the art of defect engineering.

Crystal defects can be controlled from the early beginning by influencing their formation during the crystal growth. We discussed several aspects of controlling oxygen concentration in Czochralski silicon crystals, which is the basic method for control of oxygen precipitation in silicon wafers. Defect formation can be adjusted by optimization of the crystal growth process with respect to the v/G parameter. Tuning the crystal pull rate v and the hot zone design, which determines the temperature gradient G, one can produce either silicon containing vacancy-type defects and showing enhanced oxygen precipitation or silicon containing interstitial-type defects and showing suppressed oxygen precipitation. Sometimes it can be advantageous to modify the processes of defect formation by doping of the silicon crystal with an extra element like carbon or nitrogen to promote oxygen precipitation. Since the material properties obtained by application of the above mentioned methods may not be invariable or sufficient, it may be necessary to treat also the silicon wafer.

Another reason for treatment of the wafer can be an effort to modify properties of wafer surface. For example oxygen precipitation and also appearance of the vacancy-type defects, the COPs, can be controlled by high temperature annealing of polished silicon wafers in optimized ambient. In this manner a wafer which contains a defect-free near-surface denuded zone and an optimized defect density in the bulk of the wafer providing effective gettering of metal impurities can be obtained.

We showed that various methods of defect engineering can be utilized during the growth of silicon crystals and manufacturing of wafers to produce silicon wafers of desired quality. Properties of the wafers have to be optimized for specific requirements of individual types of electronic devices and integrated circuits. Following the development of electronic industry, engineering of crystal defects remains an inseparable and never-ending part of the silicon manufacturing technology.

9. Acknowledgment

This work was partially supported by grant FR-TI3/031 awarded by the Ministry of Industry and Trade of the Czech Republic. Critical reading of the manuscript by Dr. John M. Parsey, Jr., is highly acknowledged.

10. References

Abe, T.; Harada, H. & Chikawa, J. (1983). Swirl Defects in Float-Zoned Silicon Crystals, *Physica B+C*, Vol. 116, No. 1-3, (February 1983), pp. 139-147, ISSN 0378-4363

Adachi, N.; Hisatomi, T.; Sano, M.; & Tsuya, H. (1998). Reduction of Grown-in Defects By High Temperature Annealing, In: *Semiconductor Silicon 1998*, Huff, H.R.; Gösele, U.; Tsuya, H. (Eds.), pp. 698-706, The Electrochemical Society, ISBN 978-1-56677-193-1698, Penington, NJ, USA

Andrews, J. (1983). Oxygen Out-Diffusion Model for Denuded Zone Formation in Czochralski-Grown Silicon with High Intersitital Oxygen Content, In: Defects in Silicon, Murray Bullis, W. & Kimerling, L. C. (Eds.), pp. 133-141, The Electrochemical Society, Pennington, NJ

ASTM Standard F1188-02 (2003). *Standard Test Method for Interstitial Atomic Oxygen Content of Silicon by Infrared Absorption with Short Baseline*, ASTM International, West Conshohocken, PA, USA

ASTM standard F 1809–02 (2003), *Standard Guide for Selection and Use of Etching Solutions to Delineate Structural Defects in Silicon*, ASTM International, West Conshohocken, PA, USA

Borghesi, A.; Pivac, B.; Sassella, A. & Stella, A. (1995). Oxygen Precipitation in Silicon, *Journal of Applied Physics*, Vol. 77, No. 9, (May 1995), pp. 4169-4244. ISSN 0021-8979

Borionetti, G.; Gambaro, D.; Porrini, M. & Voronkov, V.V. (2002). In: *Semiconductor Silicon 2002*, Huff, H.R.; Fabry, L. & Kishino S. (Ed.), pp. 505-516, The Electrochemical Society, ISBN 1-56677-374-1, Penington, NJ, USA

Bullis, W.M. (1990). Silicon Material Properties, In: *Handbook of Silicon Technology*, O´Mara, W.C.; Herring R.P.; & Hunt, L.P., (Eds.), 347-450, Noyes Publications, ISBN 0-8155-1237-6, Park Ridge, NJ, USA

Brown, R.A.; Wang, Z. & Mori, T. (2001). Engineering Analysis of Microdefect Formation During Silicon Crystal Growth, *Journal of Crystal Growth*, Vol. 225, No. 2-4, (May 2001), pp. 97-109, ISSN 0022-0248

Czochralski, J. (1918). Ein neues Verfahren zur Messung des Kristallisationsgeschwindigkeit der Metalle, *Zeitschrift für Physikalische Chemie*, Vol. 92, (1918), pp. 219-221

Dupret, F. & Van den Bogaert, N. (1994). Modelling Bridgman and Czochralski growth, In: *Handbook of Crystal Growth*, Vol. 2B, Chapter 15, Hurle, D.T.J. (Ed.), 875-1010, North Holland / Elsevier, ISBN 0-444-81554-6, Amsterodam, Holand

Falster, R.; Gambaro, D.; Olmo, M.; Cornara, M. & Korb, H. (1998). The Engineering of Silicon Wafer Material Properties Through Vacancy Concentration Profile Control and the Achievement of Ideal Oxygen Precipitation Behavior, *Material Research Society Syposium Proceedings*, Vol. 510, pp. 27-36, ISSSN 0272-9172

Föll, H. & Kolbesen, B.O. (1975). Formation and Nature of Swirl Defects in Silicon. *APPLIED PHYSICS A: MATERIAL SCIENCE AND PROCESSING*, Vol. 8, No. 4, (December 1975), pp. 319- 331, ISSN 0947-8396

Graff, K. (2000). *Metal Impurities in Silicon-device Fabrication* (Second, Revised Edition), Springer-Verlag Berlin Heidelberg New York, ISBN 3-540-64213-7, Berlin, Germany

Ham, F.S. (1958). Theory of Diffusion-Limited Precipitation, *Journal of Physics and Chemistry of Solids*, Vol. 6, No. 4, (September 1958), pp. 335-351, ISSN 0022-3697

Hasebe, M. Takeoka, Y. Shinoyama S. & Naito S. (1989), Formation Process of Stacking Faults with Ringlike Distribution in CZ-Si Wafers, *Japanese Journal of Applied Physics*, Vol. 28, No. 11, (January 1980), pp. L1999-L2002, ISSN 0021-4922

Hirth, J.P. & Lothe, J. (1967). *Theory of dislocations*, McGraw-Hill, ISBN 0-521-86436-4, New-York, US

Hurle, D.T.J. (1993). *Crystal Pulling from the Melt*, Springer-Verlag Berlin-Heidelberg New York, ISBN 3-540-56676-7, Berlin, Germany

Ikari, A.; Nakai, K.; Tachikawa, Y.; Deai, H.; Hideki, Y.; Ohta, Y.; Masahashi, N.; Hayashi, S.; Hoshino, T. & Ohashi, W. (1999). Defect Control in Nitrogen Doped Czochralski Silicon Crystals, *Solid State Phenomena*, Vol. 69-70 (1999), pp. 161-166, ISSN ISSN 1662-9779

Itsumi, M. (2002). Octahedral Void Defects in Czochralski Silicon, *Journal of Crystal Growth*, Vol. 237-239, No. 3 (April 2002), pp. 1773-1778, ISSN 0022-0248

Kalaev, V.V.; Lukanin, D.P.; Zabelin, V.A.; Makarov, Yu.N.; Virbulis, J.; Dornberger, E. & von Ammon, W. (2003), *Materials Science in Semiconductor Processing*, Vol. 5, No. 4-5, (August-October 2003), pp. 369–373, ISSN 1369-8001

Keck, P.H. & Golay, M.J.E. (1953), Crystallization of Silicon from a Floating Liquid Zone, *Physical Review*, Vol. 89, (March 1953), pp. 1297

Lang, A. R. (1978), Techniques and interpretation in X-ray topography. In: *Diffraction and Imaging Techniques in Materials Science*, Amelinckx, S.; Gevers, R. & Van Landuyt, J. (Eds.), 2nd ed. rev. (1978), pp 623–714, North-Holland, ISBN 9780444851307, Amsterdam, Holand

Nadahara, S.; Kubota, H. & Samata, S. (1997). Hydrogen Annealed Silicon Wafer, *Solid State Phenomena*, Vol. 57-58 (1997), pp. 19-26, ISSN 1662-9779

Nagasawa, K.; Matsushita, Y. & Kishino, S. (1980). A New Intrinsic Gettering Technique Using Microdefects in Czochralski Silicon Crystal: A New Double Preannealing Technique, *Applied Physics Letters*, Vol. 37, No. 7, (October 1980), pp. 622-624, ISSN 0003-6951

O´Mara, W.C. (1990). Oxygen, Carbon and Nitrogen in Silicon, In: *Handbook of Silicon Technology*, O´Mara, W.C.; Herring R.P.; & Hunt, L.P., (Eds.), pp. 451-549, Noyes Publications, ISBN 0-8155-1237-6, Park Ridge, NJ, USA

Pichler, P. (2004). *Intrinsic Point Defects, Impurities, and Their diffusion in Silicon*, Springer-Verlag Wien New York, ISBN 3-211-20687-6, Wien, Austria

Ravi, K.V. & Varker, C.J. (1974). Oxidation-Induced Stacking Faults in Silicon. I. Nucleation phenomenon, *Journal of Applied Physics*, Vol. 45, No. 1, (January 1974), pp. 263-271, ISSN 0021-8979

Roksnoer, P.J. & van den Boom, M.M.B. (1981). Microdefects in a Non-Striated Distribution in Floating-Zone Silicon Crystals. *Journal of Crystal Growth.* Vol. 53, No. 3, (June 1981), pp. 563- 573, ISSN 0022-0248.

Rozgonyi, G.A.; Deysher, R.P. & Pearce, C.W. (1976). The Identification, Annihilation, and Suppression of Nucleation Sites Responsible for Silicon Epitaxial Stacking Faults, *Journal of The Electrochemical Society*, Vol. 123, No. 12, (December 1976), pp. 1910-1915, ISSN 0013-4651.

Ryuta, J.; Morita, E.; Tanaka, T. & Shimanuki, Y. (1990). Crystal-Originated Singularities on Si Wafer Surface after SC1 Cleaning, *Japanese Journal of Applied Physics*, Vol. 29, No. 10, (October 1990), pp. L1947-L1949, ISSN 0021-4922

Schröder, D.K. (1989). Lifetime in Silicon, In: *Gettering and Defect Engineering in the Semiconductor Technology*, Kittler, M. (Ed.), pp. 383-394, Sci-Tech, ISBN 3-908044-04-9, Vaduz, FL

Shimura, F. (1994). *Oxygen in Silicon*, Academic Press, ISBN 0-127-52142-9, London, UK

Sumino, K.; Harada, H. & Yonenaga, I. (1980). The Origin of the Difference in the Mechanical Strengths of Czochralski-Grown Silicon and Float-Zone-Grown Silicon, *Japanese Journal of Applied Physics*, Vol. 19, No. 1, (January 1980), pp. L49-L52, ISSN 0021-4922

Teal, G.K. & Little, J.B. (1950). Growth of Germanium Single Crystals, *Physical Review*, Vol. 78, (1950), pp 647

Válek, L.; Lysáček, D. & Šik, J. (2007). OISF Pattern and Grown-in Precipitates in Heavily Boron Doped Silicon, *Journal of The Electrochemical Society*, Vol. 154, No. 10 (August 2007), pp H904-H909, ISSN 0013-4651

Válek, L.; Šik, J. & Lysáček, D. (2008). Enhanced Oxygen Precipitation during the Czochralski Crystal Growth, *Solid State Phenomena*, Vol. 131-133, (2008), pp. 167-174, ISSN 1662-9779

Vanhellemont, J.; Senkader, S.; Kissinger, G.; Higgs, V.; Trauwaert, M.-A.; Graef, D.; Lambert, U. & Wagner, P. (1997). Measurement, Modelling and Simulation of Defects in As-grown Czochralski Silicon, *Journal of Crystal Growth*, Vol. 180, No. 3-4 (October 1997), pp. 353-362, ISSN 0022-0248

von Ammon, W.; Dornberger, E. & Hansson, P.O. (1999). Bulk properties of very large diameter silicon single crystals, *Journal of Crystal Growth*, Vol. 198/199, No. 1, (March 1999), pp. 390-398, ISSN 0022-0248

von Ammon, W.; Holzl, R.; Virbulis, J.; Dornberger, E.; Schmolke, R.; Graf, D. (2001). The Impact of Nitrogen on the Defect Aggregation in Silicon, *Journal of Crystal Growth*, Vol. 226, No. 1, (June 2001), pp. 19-30, ISSN 0022-0248

Voronkov, V.V. (1982). The Mechanism of Swirl Defects Formation in Silicon, *Journal of Crystal Growth.* Vol. 59, No. 3, (October 1982), pp. 625- 643, ISSN 0022-0248.

Voronkov, V.V. (2008). Grown-in defects in silicon produced by agglomeration of vacancies and self-interstitials, *Journal of Crystal Growth*, Vol. 310, No. 7-9, (April 2008), pp. 1307-1314, ISSN 0022-0248

Yamagishi, H.; Fusegawa, I.; Fujimaki, N. & Katayama, M. (1992). Recognition of D Defects in Silicon Single Crystals by Preferential Etching and Effect on Gate Oxide Integrity, *Semiconductor Science and Technology*, Vol. 7, No. 1A, (January 1992), pp A135-A140, ISSN 0268-1242

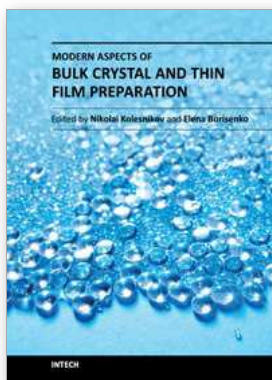

Modern Aspects of Bulk Crystal and Thin Film Preparation

Edited by Dr. Nikolai Kolesnikov

ISBN 978-953-307-610-2
Hard cover, 608 pages
Publisher InTech
Published online 13, January, 2012
Published in print edition January, 2012

In modern research and development, materials manufacturing crystal growth is known as a way to solve a wide range of technological tasks in the fabrication of materials with preset properties. This book allows a reader to gain insight into selected aspects of the field, including growth of bulk inorganic crystals, preparation of thin films, low-dimensional structures, crystallization of proteins, and other organic compounds.

How to reference

In order to correctly reference this scholarly work, feel free to copy and paste the following:

Lukáš Válek and Jan Šik (2012). Defect Engineering During Czochralski Crystal Growth and Silicon Wafer Manufacturing, Modern Aspects of Bulk Crystal and Thin Film Preparation, Dr. Nikolai Kolesnikov (Ed.), ISBN: 978-953-307-610-2, InTech, Available from: http://www.intechopen.com/books/modern-aspects-of-bulk-crystal-and-thin-film-preparation/defect-engineering-during-czochralski-crystal-growth-and-silicon-wafer-manufacturing

INTECH
open science | open minds

InTech Europe
University Campus STeP Ri
Slavka Krautzeka 83/A
51000 Rijeka, Croatia
Phone: +385 (51) 770 447
Fax: +385 (51) 686 166
www.intechopen.com

InTech China
Unit 405, Office Block, Hotel Equatorial Shanghai
No.65, Yan An Road (West), Shanghai, 200040, China
中国上海市延安西路65号上海国际贵都大饭店办公楼405单元
Phone: +86-21-62489820
Fax: +86-21-62489821

© 2012 The Author(s). Licensee IntechOpen. This is an open access article distributed under the terms of the Creative Commons Attribution 3.0 License, which permits unrestricted use, distribution, and reproduction in any medium, provided the original work is properly cited.